© 2014. Published by The Company of Biologists Ltd | Journal of Cell Science (2014) 000, 000–000 doi:10.1242/jcs.164293

CORRECTION

Ultrastructural analysis of autophagosome organization using mammalian autophagy-deficient cells

Chieko Kishi-Itakura, Ikuko Koyama-Honda, Eisuke Itakura and Noboru Mizushima

There was an error published in *J. Cell Sci.* **127**, 4089-4102.

Daiichi-Sankyo Foundation of Life Science was omitted from the original Funding section. The complete list of funding bodies is given below.

Funding

This work was supported in part by the Funding Program for Next Generation World-Leading Researchers [grant number LS043]; Daiichi-Sankyo Foundation of Life Science; and Japan Society for the Promotion of Science (JSPS) KAKENHI Grants-in-Aid for Scientific Research on Innovative Areas [grant number 25111005] to N.M.; and grants for a research fellowship of the JSPS for Young Scientists (to E.I.); and Supporting Positive Activities for Female Researchers (to I.K.-H.).

We apologise to the readers for any confusion that this error might have caused.

© 2014. Published by The Company of Biologists Ltd | Journal of Cell Science (2014) 127, 4089–4102 doi:10.1242/jcs.156034

RESEARCH ARTICLE

Ultrastructural analysis of autophagosome organization using mammalian autophagy-deficient cells

Chieko Kishi-Itakura[1,*], Ikuko Koyama-Honda[1,2,§], Eisuke Itakura[1,‡,§] and Noboru Mizushima[1,2,¶]

ABSTRACT

Autophagy is mediated by a unique organelle, the autophagosome. Autophagosome formation involves a number of autophagy-related (ATG) proteins and complicated membrane dynamics. Although the hierarchical relationships of ATG proteins have been investigated, how individual ATG proteins or their complexes contribute to the organization of the autophagic membrane remains largely unknown. Here, systematic ultrastructural analysis of mouse embryonic fibroblasts (MEFs) and HeLa cells deficient in various ATG proteins reveals that the emergence of the isolation membrane (phagophore) requires FIP200 (also known as RB1CC1), ATG9A and phosphatidylinositol (PtdIns) 3-kinase activity. By contrast, small premature isolation-membrane-like and autophagosome-like structures were generated in cells lacking VMP1 and both ATG2A and ATG2B, respectively. The isolation membranes could elongate in cells lacking ATG5, but did not mature into autophagosomes. We also found that ferritin clusters accumulated at the autophagosome formation site together with p62 (also known as SQSTM1) in autophagy-deficient cells. These results reveal the specific functions of these representative ATG proteins in autophagic membrane organization and ATG-independent recruitment of ferritin to the site of autophagosome formation.

KEY WORDS: Autophagosome, ATG, Ferritin, p62, SQSTM1

INTRODUCTION

The lysosome is a cellular organelle that contains acid hydrolases to degrade delivered materials. Autophagy is a major trafficking pathway required to transfer cytoplasmic materials into the lysosome (Mizushima et al., 2011; Tooze and Yoshimori, 2010). Macroautophagy (hereafter, referred to simply as autophagy) is mediated by a double-membraned structure, the autophagosome, which is generated on or near the endoplasmic reticulum (ER) by the expansion of a membrane sac structure termed the isolation membrane or phagophore. Sealing the edge of the isolation membrane generates the autophagosome, which contains the cytoplasmic materials. Fusion between the outer autophagosomal and lysosomal membranes leads to the degradation of the enclosed materials. Autophagy is important for many physiological processes, such as the generation of amino acids under starvation conditions, cytoplasmic quality control, early embryogenesis, tumor suppression, elimination of bacteria and prevention of various diseases (Choi et al., 2013; Levine and Kroemer, 2008; Mizushima and Komatsu, 2011).

Autophagosome formation is governed by a set of autophagy-related (ATG) proteins, which are highly conserved among eukaryotes (Lamb et al., 2013; Mizushima et al., 2011; Nakatogawa et al., 2009). In mammals, upon induction of autophagy – for example, by starvation – both a complex containing ULK, ATG13, FIP200 (also known as RB1CC1) and ATG101, and ATG9A-containing vesicles are independently recruited to the autophagosome formation site, where they then recruit the ATG14–Beclin-1–VPS34–VPS15 complex. This is a class III phosphatidylinositol (PtdIns) 3-kinase complex that generates phosphatidylinositol 3-phosphate [PtdIns(3)P] on the ER membrane or closely associated autophagic precursors. Downstream of these factors, PtdIns(3)P effectors – such as double FYVE-containing protein 1 (DFCP1, also known as ZFYVE1) and WD-repeat protein interacting with PtdIns (WIPI) proteins – ATG2, the ATG12–ATG5–ATG16L1 complex and microtubule-associated protein light chain 3 (LC3) function to generate autophagosomes. The ER membrane protein 'vacuole membrane protein 1' (VMP1) is also thought to function at a late step of autophagosome formation (Itakura and Mizushima, 2010; Tian et al., 2010). The hierarchical relationship among these ATG proteins in recruitment to the yeast pre-autophagosomal structure (Suzuki et al., 2007) and the mammalian autophagosome formation site (Itakura and Mizushima, 2010), and the temporal order of their recruitment have been determined (Koyama-Honda et al., 2013). However, how each factor or complex contributes to the organization of the autophagic membrane has not yet been systematically analyzed, even in yeast cells.

Here, we performed ultrastructural analysis of mammalian cells deficient in representative ATG proteins, including FIP200, ATG9A, ATG2A and ATG2B, VMP1 and ATG5, and found that the emergence of the isolation membrane required FIP200, ATG9A and PtdIns 3-kinase activity. By contrast, small premature isolation-membrane-like or autophagosome-like structures were generated in cells lacking both ATG2A and ATG2B or VMP1, respectively. Isolation membranes could elongate in cells lacking ATG5, but they did not mature into autophagosomes. We also found that ferritin clusters accumulate at the autophagosome formation site together with p62 (also known as SQSTM1) in autophagy-deficient cells. This study reveals the specific function of each ATG protein in autophagic membrane dynamics and identifies ferritin as a novel selective substrate that translocates to the autophagosome formation site.

[1]Department of Physiology and Cell Biology, Tokyo Medical and Dental University, Tokyo 113-8519, Japan. [2]Department of Biochemistry and Molecular Biology, Graduate School and Faculty of Medicine, The University of Tokyo, Tokyo 113-0033, Japan.
*Present address: Cambridge Institute for Medical Research, University of Cambridge, Cambridge CB2 0XY, UK. ‡Present address: MRC Laboratory of Molecular Biology, Cambridge CB2 0QH, UK
§These authors contributed equally to this work

¶Author for correspondence (nmizu@m.u-tokyo.ac.jp)

Received 2 May 2014; Accepted 3 July 2014

Journal of Cell Science (2014) 127, 4089–4102 doi:10.1242/jcs.156034

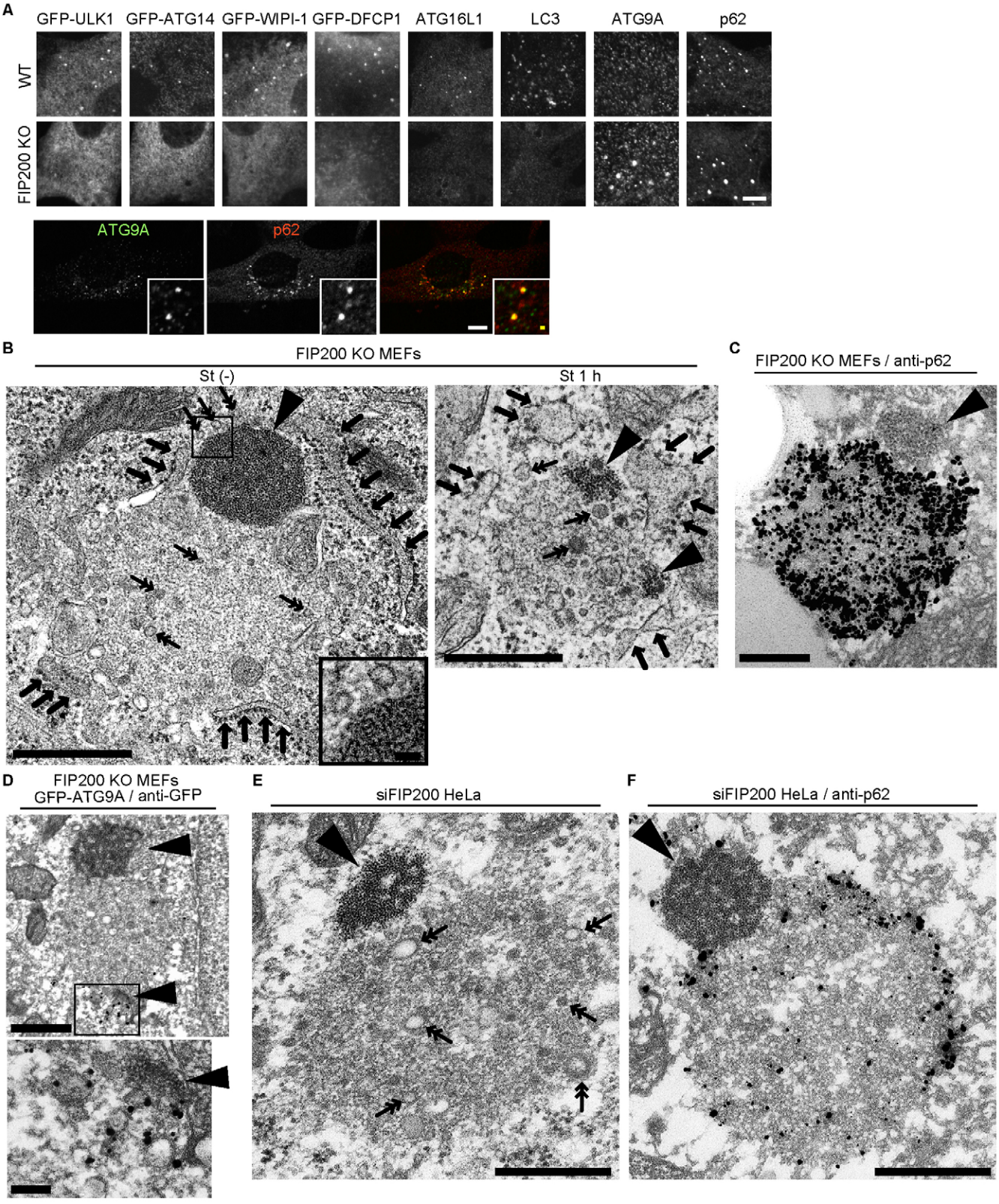

Fig. 1. See next page for legend.

RESULTS

Emergence of the isolation membrane requires FIP200 and ATG9A

We systematically analyzed the morphology of autophagy-related structures in various autophagy-deficient cells. In wild-type mouse embryonic fibroblasts (MEFs), upstream ATG proteins (such as ULK1, ATG14, WIPI-1, DFCP1 and ATG16L1) and LC3 formed punctate structures (Fig. 1A), which represented isolation membranes and pan-autophagic membranes as described previously (Lamb et al., 2013; Mizushima et al., 2010). One of

Journal of Cell Science (2014) 127, 4089–4102 doi:10.1242/jcs.156034

Fig. 1. FIP200-deficient cells show accumulation of selective autophagic substrates but no isolation membranes. (A) Wild-type (WT) and FIP200-knockout (KO) MEFs with or without stable expression of the indicated constructs were cultured in starvation (St) medium for 1–2 h and subjected to fluorescence microscopy. Endogenous ATG16L1, LC3, ATG9A and p62 were stained. Scale bars: 10 μm (white), 1 μm (yellow). (B–F) FIP200-knockout MEFs under growth conditions (B), and FIP200-knockout MEFs (C), FIP200-knockout MEFs expressing GFP–ATG9A (D) and HeLa cells treated with siRNA against FIP200 (E,F) under starvation conditions for 1 h were fixed and subjected to conventional electron microscopy (B,E) and immunoelectron microscopy using anti-p62 (C,F) and anti-GFP antibodies (D). A magnified image of the high-density cluster is shown in the inset in B. Arrowheads, clusters of high-density particles; arrows, ER surrounding the ribosome-free area; double-headed arrows, vesicles inside and at the periphery of the ribosome-free area. Scale bars: 500 nm [B,D (upper panel),E,F], 50 nm (B, inset), 200 nm (C), 100 nm [D (lower panel)].

the best-characterized selective substrates of autophagy, p62, is known to colocalize with LC3 through direct binding (Birgisdottir et al., 2013). ATG9A showed a number of small punctate structures, most of which represented 'ATG9 vesicles' (Itakura et al., 2012a; Orsi et al., 2012). In MEFs lacking FIP200, which is essential for an initial step in autophagosome formation (Hara et al., 2008), these ATG proteins (except ATG9A) did not form punctate structures (Itakura and Mizushima, 2010), although some LC3 puncta were occasionally found (Hara et al., 2008; Itakura and Mizushima, 2010), and only ATG9A and p62 accumulated in clear punctate structures (Fig. 1A). Based on our previous observation that p62 colocalizes very well with not only ATG9A but also VMP1 in FIP200-knockout MEFs, these structures should represent the autophagosome formation sites (Itakura et al., 2012a; Itakura and Mizushima, 2011) (Fig. 1A).

Electron microscopy frequently showed unique structures in the cytoplasm of FIP200-knockout MEFs under both growth (regular) and starvation conditions (Fig. 1B). These structures consisted of ribosome-free areas surrounded by the ER (Fig. 1B, arrows). Some vesicles (~10–70 nm in diameter) were observed inside and at the periphery of the ribosome-free area (Fig. 1B, double-headed arrows). These areas were often associated with one or a few large clusters (~100–500 nm in diameter) of high-density small particles (Fig. 1B, arrowheads and inset). We observed approximately five such structures (combination of the ER, ribosome-free areas, vesicles and high-density particle clusters) in one cell from an ultrathin section of FIP200-knockout MEFs. Isolation-membrane-like structures were not detected.

In these complex structures, p62 was detected in the ribosome-free area by immunoelectron microscopy (Fig. 1C). Notably, p62 was completely lacking in the clusters of high-density particles, which were essentially absent from wild-type MEFs, implying that they might be novel selective substrates of autophagy accumulated in autophagy-deficient cells. Immunoelectron microscopy also showed that at least some of the vesicles, which accumulated mainly at the periphery of the p62 area, were ATG9A positive (Fig. 1D). The presence of both p62 and ATG9A suggests that this region in fact represents the autophagosome formation site. Also, similar structures (p62 aggregates, small vesicles and high-density particle clusters, but no isolation membranes) were observed in FIP200-knockdown HeLa cells by conventional electron microscopy (Fig. 1E) and p62 immunoelectron microscopy (Fig. 1F), suggesting that these are not specific to MEFs.

ATG9A is another upstream autophagy factor required for recruitment of most ATG proteins, except the ULK–FIP200 complex (Fig. 2A) (Itakura et al., 2012a; Orsi et al., 2012). ULK1 consistently colocalized with p62 in ATG9-knockout MEFs (Fig. 2A). Electron microscopy analysis of ATG9-knockout MEFs (Fig. 2B) and ATG9A-knockdown HeLa cells (Fig. 2C,D) showed the presence of p62 aggregates, small vesicles and high-density particle clusters (sometimes with hollows), which were similar to the structures observed in FIP200-deficient cells (Fig. 1). ULK1 signals, which were associated with elongating isolation membranes in wild-type cells, were detected mainly around the high-density clusters and, in some cases, around the p62 aggregates, but not on the surrounding ER, in ATG9A-knockout MEFs (Fig. 2E). This suggests that ULK1 translocates to some unknown structures rather than the ER itself during isolation membrane formation. Again, isolation-membrane-like structures were not detected in these ATG9A-deficient cells.

These data suggest that FIP200 and ATG9A are essential for the emergence of the isolation membrane and that, in their absence, p62 aggregates, small vesicles (including ATG9 vesicles, at least in FIP200-deficient cells) and unknown high-density clusters accumulate at the autophagosome formation site.

The high-density particle clustered at the autophagosome formation site is ferritin

The unknown clusters at the autophagosome formation site in FIP200- and ATG9A-deficient cells contained a large number of small high-density particles with a diameter of ~10 nm (Fig. 1B, inset). After extensive literature searching for similar structures, we identified the high-density particle as ferritin. Ferritin is an iron storage and detoxification protein, and ferritin proteins assemble into a shell, which is a hollow spherical complex of 24 subunits (consisting of a mixture of H- and L-ferritins) with an external diameter of 12 nm (Arosio et al., 2009; Watt, 2011). Ferritin shells are diffusely present in the cytoplasm under normal conditions, but can be deposited as clusters in certain settings, such as in normal rat erythroblasts and reticulocytes (Heynen and Verwilghen, 1982) and in erythroblasts in patients with sideroblastic anemia, in which iron accumulates due to inefficient hemoglobin synthesis (Ghadially, 1975). The ultrastructure of these ferritin deposits is quite similar to that of the high-density clusters that we observed in FIP200-knockout and ATG9A-knockout MEFs.

To confirm that the high-density particles are indeed ferritin, we stained wild-type, FIP200-knockout and ATG9A-knockout MEFs with anti-ferritin antibody. In wild-type MEFs, ferritin formed many small puncta, which did not colocalize with p62 (Fig. 3A). However, in FIP200-knockout and ATG9A-knockout MEFs, ferritin formed brighter punctate structures, which were in close proximity to the p62 puncta (Fig. 3A). Such a close association between ferritin and p62 was also observed in ATG9A-siRNA-treated HeLa cells (Fig. 3B). Furthermore, we performed immunoelectron microscopy using anti-ferritin antibody and confirmed that the high-density particles observed in ATG9A-knockout MEFs (Fig. 3Ca,b) and in ATG9A-silenced HeLa cells (Fig. 3Cc,d) were ferritin. The ferritin signals were detected mainly on the surface of the large clusters. Because we used a pre-embedding immunogold labeling method, the results suggest that the ferritin clusters are tightly packed structures that impede antibody penetration. Consistent with the electron microscopy data shown in Fig. 2E, GFP–ULK1 puncta were well colocalized with the ferritin signals in ATG9A-knockout

Journal of Cell Science (2014) 127, 4089–4102 doi:10.1242/jcs.156034

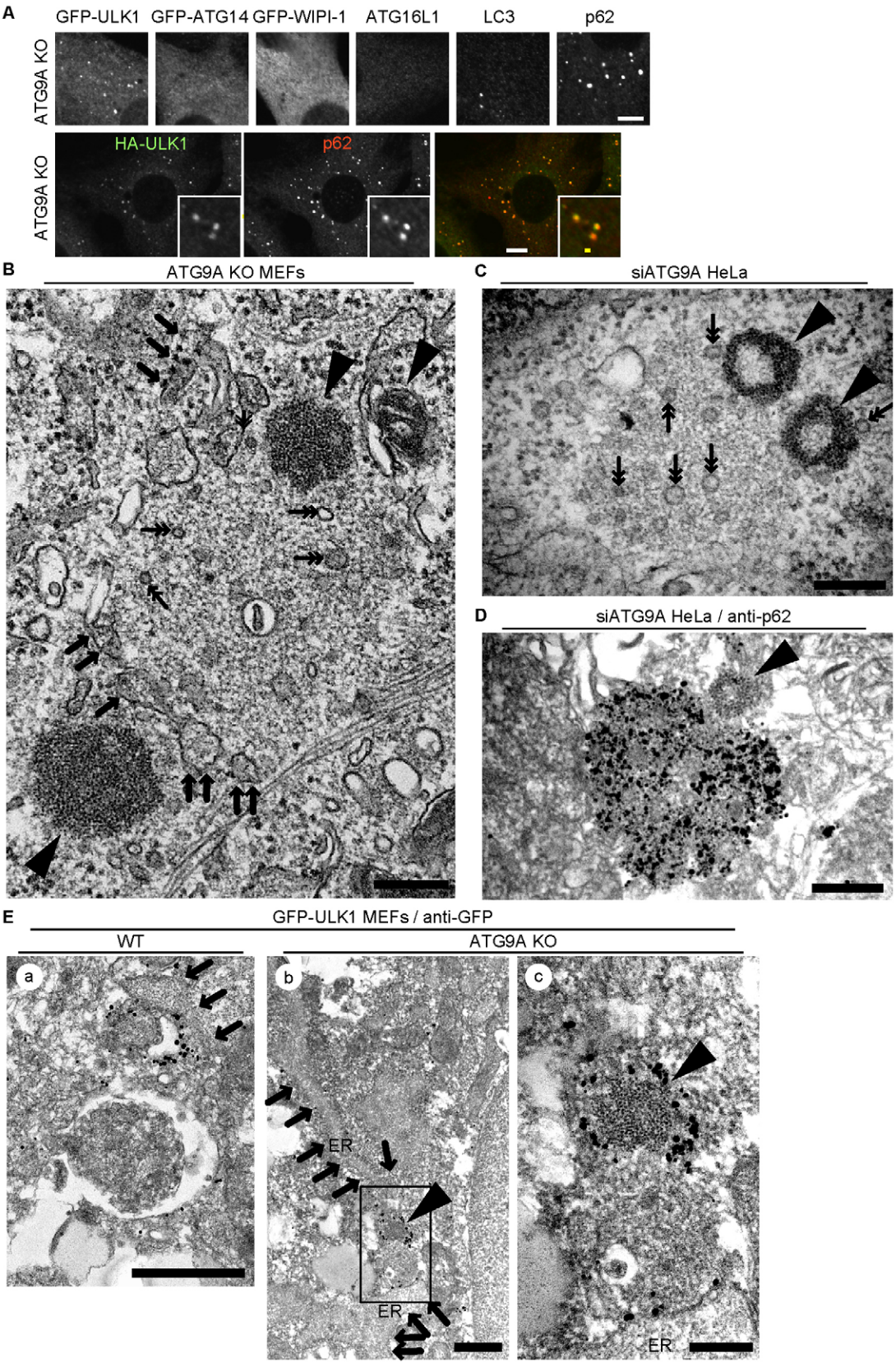

Fig. 2. ATG9A-deficient cells show structures similar to those observed in FIP200-deficient cells. (A) ATG9A-knockout (KO) MEFs with or without stable expression of the indicated constructs were cultured in starvation medium for 1–2 h and subjected to fluorescence microscopy. Endogenous ATG16L1, LC3 and p62 were stained. Scale bars: 10 μm, 1 μm (inset). (B–E) ATG9A-knockout MEFs (B), HeLa cells treated with siRNA against ATG9A (C,D) and wild-type (WT) (Ea) and ATG9A-knockout (Eb,c) MEFs expressing GFP–ULK1 were cultured in starvation medium for 1 h and subjected to conventional electron microscopy (B,C) and immunoelectron microscopy using anti-p62 (D) and anti-GFP (E) antibodies. Arrowheads, clusters of high-density particles; arrows, ER surrounding the ribosome-free area; double-headed arrows, vesicles inside and at the periphery of the ribosome-free area. Scale bars: 500 nm (Ea,b), 200 nm (B–D,Ec).

Journal of Cell Science (2014) 127, 4089–4102 doi:10.1242/jcs.156034

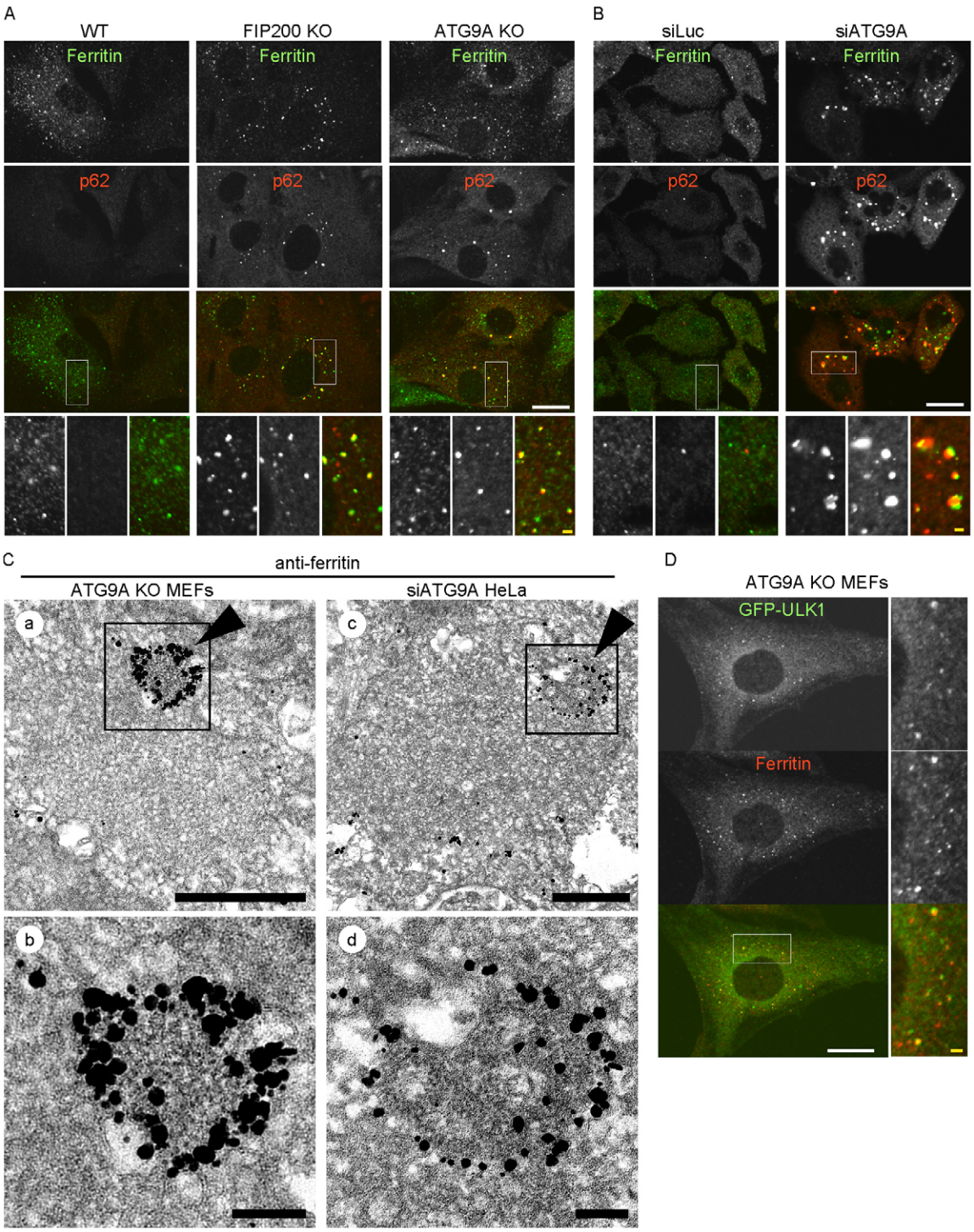

Fig. 3. The high-density particle clustered at the autophagosome formation site is ferritin. (A,B) Wild-type (WT), FIP200-knockout (KO) and ATG9A-knockout MEFs (A) and HeLa cells treated with oligos against ATG9A or control oligos (luciferase, siLuc) (B) were cultured in regular medium. Cells were stained with anti-ferritin (green) and anti-p62 (red) antibodies. Scale bars: 10 μm (white), 1 μm (yellow). (C) ATG9A-knockout MEFs (a,b) and HeLa cells treated with siRNA against ATG9A (c,d) were cultured in starvation medium for 1 h and subjected to immunoelectron microscopy using an anti-ferritin antibody. Panels b and d show magnified images of the indicated areas in panels a and c, respectively. Scale bars: 500 nm (a,c), 100 nm (b,d). Arrowheads, ferritin-positive high-density particle clusters. (D) ATG9A-knockout MEFs stably expressing GFP–ULK1 cultured in regular medium were analyzed by immunocytochemistry using anti-GFP (green) and anti-ferritin (red) antibodies. Scale bars: 10 μm (white), 1 μm (yellow).

Journal of Cell Science (2014) 127, 4089–4102 doi:10.1242/jcs.156034

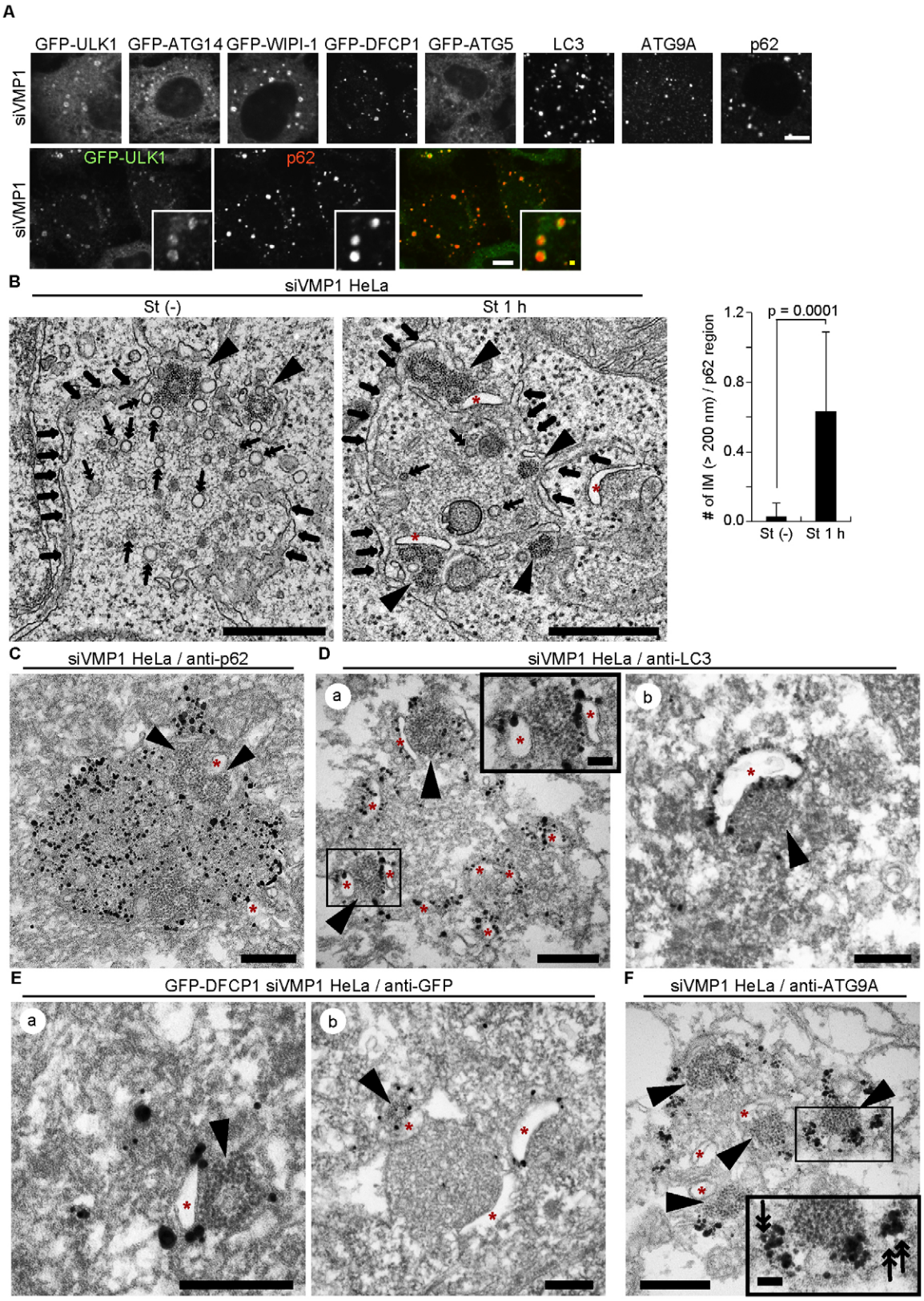

Fig. 4. See next page for legend.

Fig. 4. Accumulation of small isolation-membrane-like structures in VMP1-silenced cells. (A) HeLa cells treated with siRNA against VMP1 with or without stable expression of the indicated constructs were cultured in starvation medium for 1–2 h and subjected to fluorescence microscopy. Endogenous ATG9A, LC3 and p62 (red) were stained. Scale bars: 10 μm (white); 1 μm (yellow). (B–F) HeLa cells treated with siRNA against VMP1 with (E) or without (B–D,F) stable expression of GFP–DFCP1 were cultured in regular (B) or starvation (St) medium (B–F) for 1 h and subjected to conventional electron microscopy (B) and immunoelectron microscopy using anti-p62 (C), anti-LC3 (D), anti-GFP (E) and anti-ATG9A antibodies (F). Arrowheads, ferritin clusters; arrows, ER surrounding the ribosome-free area; double-headed arrows, vesicles inside and at the periphery of the ribosome-free area; asterisks, small isolation membrane (IM)-like structures. The graph in B indicates the number of isolation-membrane-like structures (longer than 200 nm) per p62-positive region. Data are presented as the mean±s.e.m. of 37 [growth, St (-)] and 57 [starvation, St 1 h] p62-positive regions. Scale bars: 500 nm (B), 200 nm (C–F), 50 nm (D,F, inset).

MEFs (Fig. 3D). These data demonstrate that defects in autophagy lead to the assembly of not only p62 but also ferritin at the autophagosome formation site.

Emergence of the isolation membrane requires PtdIns 3-kinase activity

As both the ULK1 complex and ATG9A are required for recruitment of the autophagy-specific PtdIns 3-kinase complex, we observed structures accumulating at the autophagosome formation sites in cells treated with wortmannin, a specific inhibitor of PtdIns 3-kinase. In cells cultured in growth medium without wortmannin, ATG9A and ULK1 rarely colocalized with each other. However, both formed bright puncta and mostly colocalized in wortmannin-treated starved cells, as previously reported (supplementary material Fig. S1A) (Itakura et al., 2012a). p62 and ferritin were also recruited to these punctate structures (supplementary material Fig. S1A).

By electron microscopy, aggregated structures associated with the surrounding ER, small vesicles and ferritin clusters were observed in wortmannin-treated starved HeLa cells (supplementary material Fig. S1B). However, as in FIP200-knockout and ATG9A-knockout cells, no isolation membrane generation was detected, suggesting that, like FIP200 and ATG9A, PtdIns 3-kinase activity is essential for isolation membrane formation.

VMP1 and ATG2 are required for elongation and development of the isolation membrane

Next, we investigated the autophagic structures in VMP1- and ATG2-deficient cells, which show similar phenotypes by fluorescence microscopy; almost all ATG proteins accumulated at the autophagosome formation site (Itakura and Mizushima, 2010; Tian et al., 2010; Velikkakath et al., 2012). As previously shown, punctate structures of many ATG proteins accumulated in VMP1-silenced HeLa cells and colocalized in the same manner as that of ULK1 and p62 under nutrient-rich (data not shown) and starvation conditions (Fig. 4A). Ultrastructural analysis demonstrated that these cells, under nutrient-rich conditions, contained structures similar to those observed in FIP200- or ATG9A-deficient cells (Figs 1, 2). We observed accumulation of ribosome-free areas containing p62, small vesicles and ferritin clusters, which were surrounded by the ER (Fig. 4B,C). However, in addition to these structures, small crescent-shaped structures (~100–300 nm in length) appeared around the p62 aggregates. These crescent-shaped structures were significantly induced by starvation (Fig. 4B), were often observed in close proximity to the ferritin clusters (Fig. 4B) and were positive for LC3 (Fig. 4D). Considering that the formation of these structures was starvation dependent, we assumed that they were immature isolation membranes that could not fully elongate. Consistent with previous reports (Axe et al., 2008; Uemura et al., 2014), DFCP1 signals were detected at the edge of these immature isolation membranes, suggesting that omegasome function might be maintained (Fig. 4E). In contrast to LC3 and DFCP1, ATG9A was detected on small vesicles near ferritin clusters, but not on immature isolation membranes (Fig. 4F; supplementary material Fig. S2). These data suggest that VMP1 is not essential for making immature isolation membranes but is important for their elongation or maturation.

Mammalian cells have two ATG2 homologs, ATG2A and ATG2B, which are functionally redundant (Velikkakath et al., 2012). To investigate the role of ATG2 proteins, we used HeLa cells lacking both ATG2A and ATG2B (Velikkakath et al., 2012). Although immunofluorescence studies of VMP1- and ATG2A/B-silenced cells showed similar phenotypes, electron microscopy studies demonstrated a significant difference between these two cell types. Like VMP1-silenced cells, ATG2A/B-silenced cells showed accumulation of p62 aggregates, small vesicles and ferritin clusters (Fig. 5A–C). The presence of ferritin at the p62 puncta was also confirmed by immunofluorescence microscopy (Fig. 5B). However, in contrast to the above-mentioned mutant cells, ring-shaped double-membraned structures, which were ~150–300 nm in diameter, were detected inside and around the p62 aggregates in ATG2A/B-silenced cells (Fig. 5A, asterisks). Some of these contained a ferritin cluster. The number of these double-membraned structures tended to be increased under starvation conditions, although not significantly (Fig. 5A). The structures were labeled with LC3 (Fig. 5D). These features suggest that the structures are small or immature autophagosomes at an advanced stage compared with the immature isolation membranes formed in VMP1-silenced cells. It was unclear whether or not these structures were completely sealed. As in VMP1-silenced cells, ATG9A signals were mostly detected on vesicles but not on these small autophagosome-like structures (Fig. 5E). Tight contact between the ER and isolation membrane was not observed in either VMP1- or ATG2A/B-silenced cells. These data suggest that VMP1 and ATG2A/B are essential for proper elongation of the isolation membrane. Furthermore, these proteins do not have the same function; VMP1 is required for both elongation and bending (or closure) of the isolation membrane, whereas ATG2A/B appears to be required mainly for isolation membrane elongation.

ATG5 is essential for closure of the isolation membrane or acts at a late step of autophagosome formation

Accumulation of WIPI-1 and DFCP1 puncta was clearly observed in ATG5-knockout MEFs, as previously shown (Itakura and Mizushima, 2010), whereas puncta of ULK1, ATG14 (Itakura and Mizushima, 2010), ATG9A and p62 were not as obvious (Fig. 6A). ATG16L1 was observed only in the cytosol. In these cells, the morphology of isolation membranes was almost normal (Fig. 6B). Isolation membranes elongated, bent and were tightly associated with the ER. Most isolation membranes have open ends and do not show any signs of degradation. These structures were also observed in ATG5-silenced HeLa cells (Fig. 6C) and ATG3-deficient MEFs (Sou et al., 2008; Uemura et al., 2014). Occasionally, small vesicles, ribosome-free areas containing fibril aggregates and ferritin structures were also observed near

Journal of Cell Science (2014) 127, 4089–4102 doi:10.1242/jcs.156034

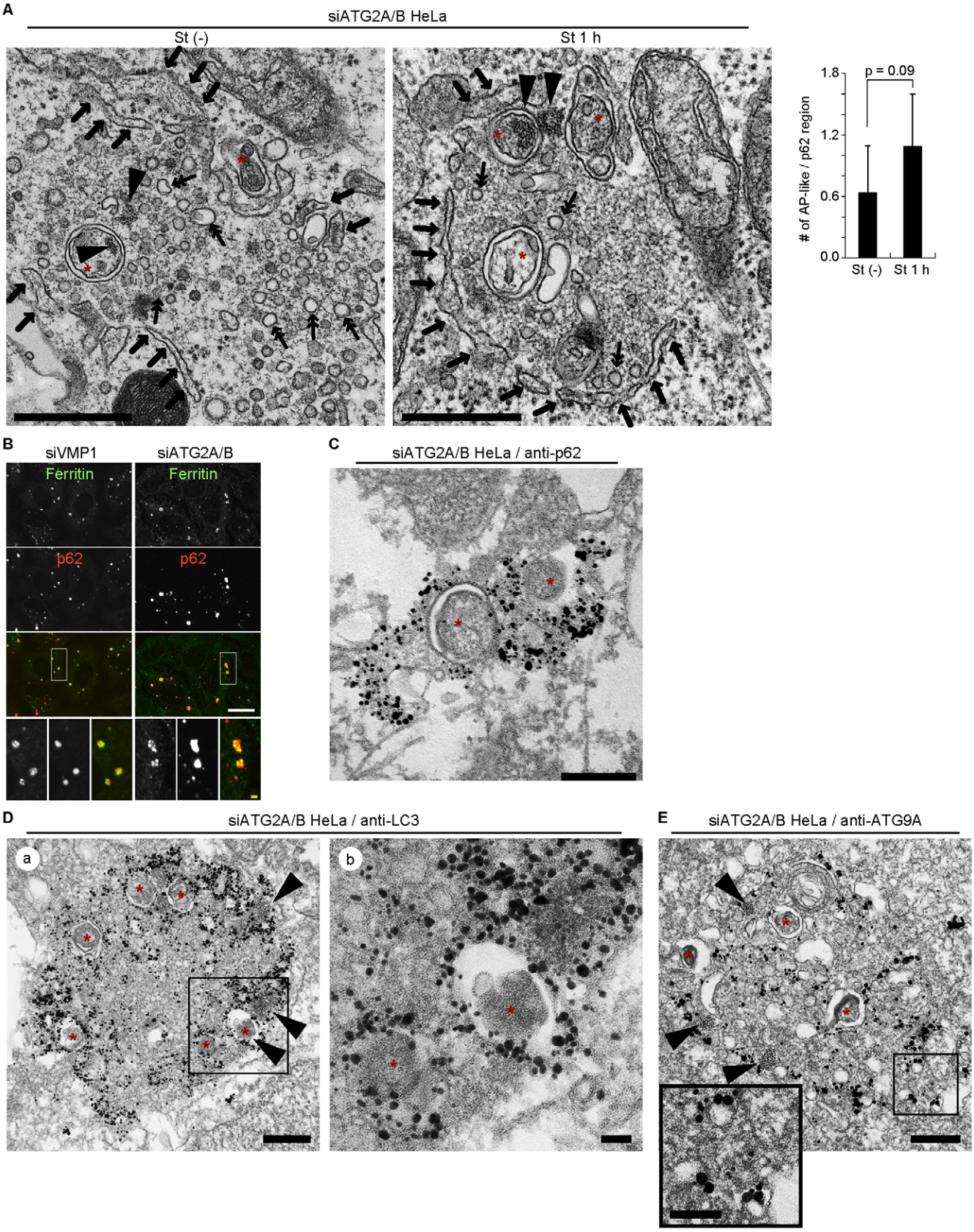

Fig. 5. See next page for legend.

Journal of Cell Science (2014) 127, 4089–4102 doi:10.1242/jcs.156034

Fig. 5. Accumulation of small autophagosome-like structures in ATG2A/B-silenced cells. (A) HeLa cells treated with siRNA against ATG2A and ATG2B were cultured in regular or starvation (St) medium for 1 h and subjected to conventional electron microscopy. The graph indicates the number of small autophagosome-like structures (asterisks) per p62-positive region. Data are presented as the mean±s.e.m. of 11 [growth, St (-)] and 46 [starvation, St 1 h] different p62-positive regions. Arrowheads, ferritin clusters; arrows, ER surrounding the ribosome-free area; double-headed arrows, vesicles inside and at the periphery of the ribosome-free area; asterisks, small autophagosome (AP)-like structures. Scale bars: 500 nm. (B) HeLa cells treated with siRNA against luciferase (data shown in Fig. 3B), VMP1 or ATG2A/B were cultured in regular medium and subjected to fluorescence microscopy. Endogenous ferritin (green) and p62 (red) were stained. Scale bars: 10 μm (white), 1 μm (yellow). (C–E) HeLa cells treated with siRNA against ATG2A/B were starved and analyzed by immunoelectron microscopy using anti-p62 (C), anti-LC3 (D) and anti-ATG9A antibodies (E). Arrowheads, ferritin clusters. Scale bars: 200 nm (C,Da,E), 50 nm (Db,E inset).

isolation-membrane-like structures, but less frequently compared with cells lacking FIP200, ATG9A, VMP1 or ATG2A/B (Fig. 6C,D). These data suggest that ATG5 is required for closure of the isolation membrane or acts at a late step of autophagosome formation.

Ferritin is selectively incorporated into autophagosomes and delivered to lysosomes

An unexpected finding is that ferritin clusters accumulate at the autophagosome formation site when autophagy is blocked, suggesting that ferritin is a selective substrate of autophagy and/or has a role in autophagosome formation. However, knockdown of both H- and L-ferritins did not affect the level of p62 or conversion of LC3-II (supplementary material Fig. S3A, panels a and b), whereas knockdown of VMP1 led to accumulation of p62 and LC3-II (supplementary material Fig. S3A, panel b). Autophagosomes with normal morphology were generated during starvation in these ferritin-knockdown cells (supplementary material Fig. S3B). Thus, it is unlikely that ferritin regulates autophagy.

Several previous studies showed that ferritin can be degraded by autophagy (Asano et al., 2011; De Domenico et al., 2009; Kidane et al., 2006; Ollinger and Roberg, 1997), and iron depletion can induce autophagy (De Domenico et al., 2009) (supplementary material Fig. S4). Yet to be determined, however, is whether ferritin is selectively incorporated into autophagosomes in wild-type cells. Upon amino acid and serum starvation, ~40% of GFP–ULK1 structures and 20% of the GFP–LC3 structures were colocalized with ferritin (Fig. 7A). These high colocalization rates were not simply due to random superposition of large amounts of ferritin puncta because these rates were significantly reduced when the colocalization assay was performed with overlaid images in which green images were artificially shifted to the right by 1 μm (Fig. 7A, triangles). Immunoelectron microscopy consistently revealed ferritin signals in degradative structures as well as in autophagosomes (Fig. 7B). These data suggest that ferritin is enriched at the autophagosome formation site and selectively incorporated into autophagosomes in wild-type cells.

Finally, we investigated the delivery of ferritin to the lysosome. Only ~10% of Lamp1-positive structures were positive for ferritin in wild-type MEFs (Fig. 7C). However, this proportion was increased to ~60% when cells were treated with protease inhibitors (E64d and pepstatin A), suggesting that ferritin is constitutively degraded in lysosomes. This colocalization rate was significantly decreased in autophagy-deficient FIP200-knockout and ATG9A-knockout MEFs, even in the presence of protease inhibitors (Fig. 7C). These findings suggest that autophagy is important for the delivery of ferritin to lysosomes.

DISCUSSION

Role of ATGs in autophagosome biogenesis

We performed ultrastructural analysis of cells deficient in ATG proteins that function at different steps in autophagosome formation. Based on our findings, we propose the following model of autophagosome biogenesis (Fig. 8). Autophagosome formation is initiated on or close to the ER, where the ULK1 complex, ATG9A vesicles and autophagy-specific PtdIns 3-kinase complex are recruited and contribute to the formation of small isolation membranes (steps I to II). Without FIP200, ATG9A and PtdIns 3-kinase activity, isolation membranes are not formed, and vesicles and selective substrates, such as p62 and ferritin clusters, accumulate and are surrounded by the ER (structure A). Small vesicles still accumulate even in ATG9A-deficient cells, suggesting that ATG9 vesicles represent only a subset of the autophagy-related vesicles or that ATG9A is not required for formation and translocation of ATG9 vesicles.

Next, small isolation membranes are properly elongated by VMP1 and ATG2A/B (steps II to III). Without VMP1, such elongation is impossible (structure B). As VMP1 primarily resides in the ER membrane (Itakura and Mizushima, 2010), the ER should contribute to the elongation step as well as the initiation step. If both ATG2A and ATG2B are deleted, the small isolation membranes can bend, but they only form small autophagosome-like structures (structure C). It is uncertain whether these structures are completely sealed and can be delivered to the lysosome. In a previous study, we showed that although autophagic flux is profoundly impaired, we could detect a small amount of protease-protected LC3-II and p62 in ATG2A/B-depleted cells (Velikkakath et al., 2012). This might indicate that a small fraction of LC3-II and p62 is sequestered inside membranous structures. Purification of these structures will further clarify the role of ATG2A/B.

Finally, the ATG12 and ATG8/LC3 conjugation systems mediate the complete closure of isolation membranes (steps III to IV). Elongated isolation membranes have been observed not only in ATG5-deficient MEFs and HeLa cells (this study, structure D), but also in ATG3-knockout MEFs (Sou et al., 2008) and ATG5-knockout embryonic stem cells (Mizushima et al., 2001). As these structures are positive for DFCP1 and WIPI, they are likely PtdIns(3)P-rich membranes. It should be noted that if these structures are cut tangentially in electron microscopy samples, they appear to be completely sealed autophagosomes. Thus, detection of these structures by electron microscopy does not itself necessarily indicate that ATG5 is not essential for macroautophagy.

Ferritin as a novel autophagy substrate

In the present study, we found that ferritin translocates to the autophagosome formation site if autophagy is blocked. Although autophagic degradation of ferritin has been suggested by the results of previous studies (Asano et al., 2011; De Domenico et al., 2009; Kidane et al., 2006; Ollinger and Roberg, 1997), in the present study we demonstrated that ferritin is a bona fide selective autophagy substrate. This could relate to the pathogenesis of static encephalopathy of childhood with neurodegeneration in adulthood (SENDA; also known as β-propeller protein-associated neurodegeneration or BPAN), a human neurodegenerative disease

Journal of Cell Science (2014) 127, 4089–4102 doi:10.1242/jcs.156034

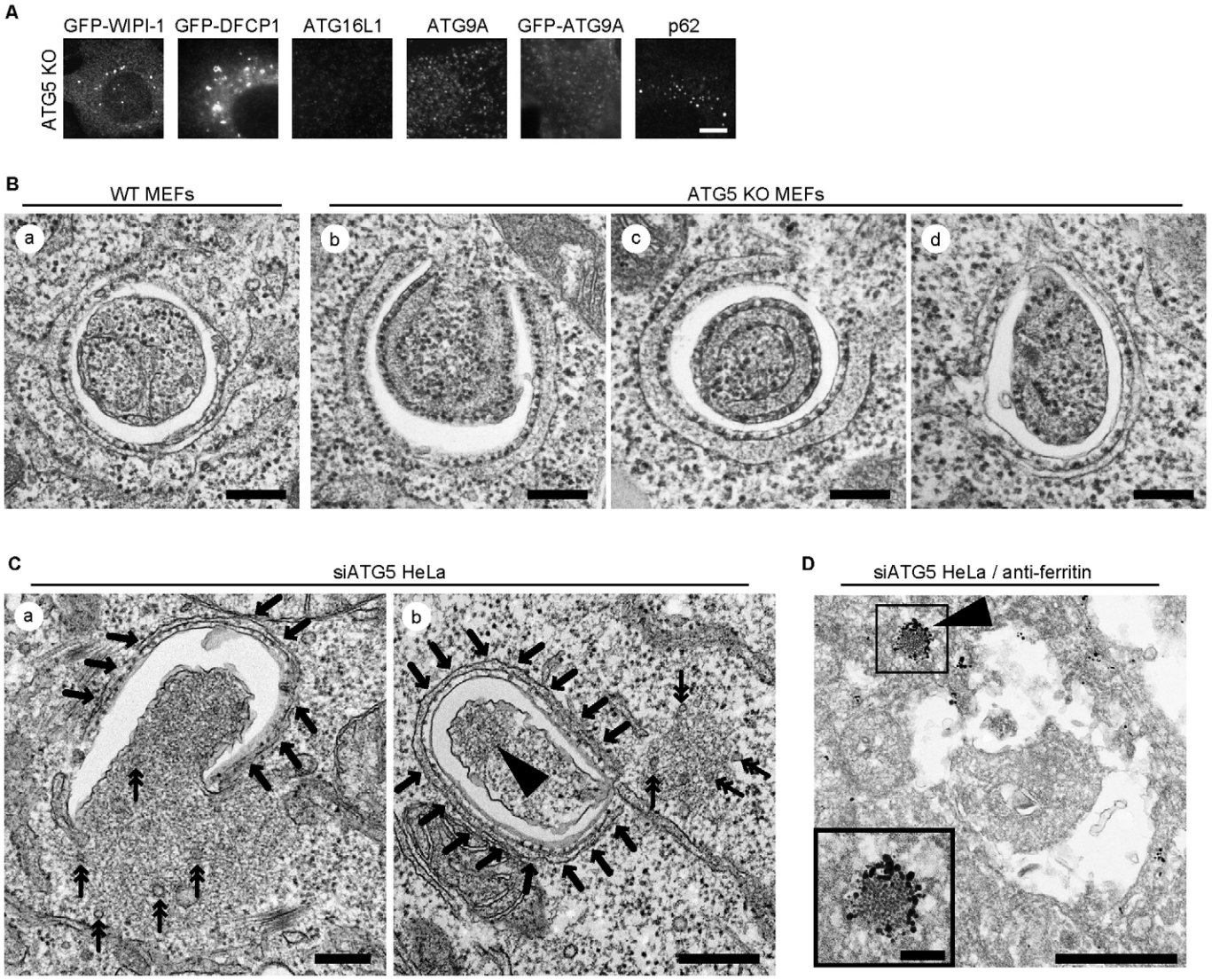

Fig. 6. Isolation membranes formed in ATG5-deficient cells. (A) ATG5-knockout (KO) MEFs with or without stable expression of the indicated constructs were cultured in starvation medium for 1 h and subjected to fluorescence microscopy. Endogenous ATG16L1, ATG9A and p62 were stained. Scale bars: 10 μm. (B–D) Wild-type (WT) and ATG5-knockout MEFs (B) and HeLa cells treated with siRNA against ATG5 (C,D) were cultured in starvation medium for 1 h and subjected to conventional electron microscopy (B,C) and immunoelectron microscopy using an anti-ferritin antibody (D). Arrowheads, ferritin clusters; arrows, ER surrounding the ribosome-free area; double-headed arrows, vesicles inside and at the periphery of the ribosome-free area. Scale bars: 200 nm (B,C), 500 nm (D), 100 nm (D, inset).

that is characterized by the accumulation of iron in the basal ganglia (Gregory and Hayflick, 2011; Haack et al., 2013). As this disease is caused by mutations in the autophagy gene *WDR45* (also known as *WIPI4*) (Haack et al., 2012; Saitsu et al., 2013), it might be due to a defect in ferritin turnover in affected neuronal cells. However, the total amount of ferritin was not increased in autophagy-deficient MEFs (data not shown) or in HeLa cells (supplementary material Fig. S3A). This could be because the intracellular ferritin concentration is tightly regulated not only at the degradation step but also at the transcriptional and translational steps. Thus, we speculate that a local increase in the ferritin concentration leads to crystallization of ferritin at the autophagosome formation site, although its physiological significance is unclear. Nonetheless, particular neuronal cell types, which show iron accumulation in SENDA/BPAN, might be more sensitive to autophagy defects compared to other cell types.

We have proposed that selective autophagy substrates, such as p62 and damaged mitochondria, can be recognized at two distinct steps: (1) LC3-independent recruitment to the autophagosome formation site and recognition by upstream ATG proteins and (2) LC3-dependent incorporation into autophagosomes (Itakura et al., 2012a; Itakura and Mizushima, 2011). Similar steps were also observed in autophagy against intracellular bacteria (Kageyama et al., 2011). The present study reveals that autophagic degradation of ferritin involves the first step; ferritin can be recruited to the autophagosome formation site in various ATG-deficient cells (e.g. FIP200 knockout and ATG9A knockout) and in wortmannin-treated wild-type cells, in which LC3 recruitment is suppressed. However, it is unclear whether the selective degradation of ferritin involves the second step. During the preparation of this manuscript, it was reported that ferritin can be incorporated into autophagosomes through interaction with

Journal of Cell Science (2014) 127, 4089–4102 doi:10.1242/jcs.156034

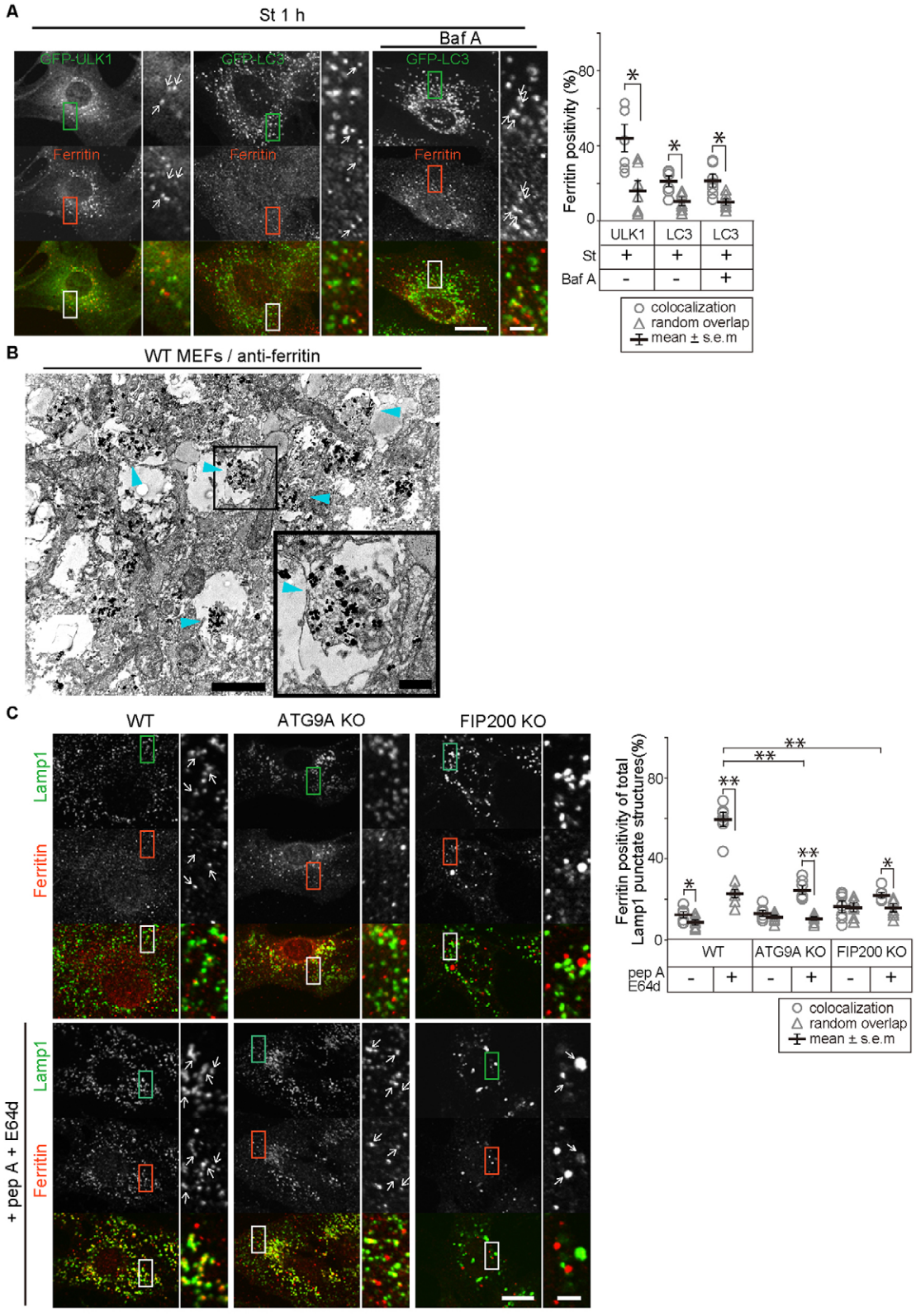

Fig. 7. See next page for legend.

NCOA4, which also binds to LC3B and GABARAPs (Mancias et al., 2014), which could be the mechanism of the second step. However, in our immunoelectron microscopy experiments, diffuse ferritin was detected inside autophagosomes but not on the inner autophagosomal membrane (Fig. 7B), indicating that ferritin might not be directly recognized by the autophagosomal membrane. This is in marked contrast to currently known autophagy substrates or adaptors, such as p62, NBR1, NDP52 (also known as

Journal of Cell Science (2014) 127, 4089–4102 doi:10.1242/jcs.156034

Fig. 7. Ferritin is selectively incorporated in autophagosomes and delivered to lysosomes. (A) MEFs stably expressing GFP–ULK1 or GFP–LC3 were cultured in starvation (St) medium with or without 100 nM bafilomycin A_1 (Baf A) for 1 h. Cells were fixed and stained with an anti-ferritin antibody and analyzed by fluorescence microscopy. The outlined areas in each image are shown at higher magnification to the right. Arrows, colocalization of GFP and ferritin signals. Scale bars: 20 μm (left), 4 μm (right). Quantification of the ferritin-positive ratio (%) of total GFP–ULK1 or GFP–LC3 punctate structures is shown in the graph (circles). Triangles represent the random overlapping ratio (%) of the colocalization (ferritin-positive ratio) (see Methods). (B) Wild-type (WT) MEFs cultured in regular medium were analyzed by immunoelectron microscopy using an anti-ferritin antibody. Arrowheads (light blue), autophagosomes. Scale bars: 500 nm, 100 nm (inset). (C) Wild-type, ATG9A-knockout (KO) and FIP200-knockout MEFs were cultured in regular medium in the presence or absence of 50 μM pepstatin (pep) A and 50 μM E64d for 24 h. Cells were fixed and stained with anti-Lamp1 and anti-ferritin antibodies, and analyzed by fluorescence microscopy. Arrows, colocalization of Lamp1 and ferritin signals. Scale bars: 20 μm (left), 4 μm (right). Quantification of the ferritin-positive ratio (%) of total Lamp1 punctate structures is shown as in A. For graphs in A and C, data represent the mean±s.e.m. (seven randomly selected cells); $*P<0.05$, $**P<0.01$; unpaired Student's *t*-test.

CALCOCO2) and Nix (also known as BNIP3L) in mammals, and Atg19 and Atg32 in yeast, which interact with LC3 and Atg8 on the autophagosomal membrane, respectively (Johansen and Lamark, 2011; Noda et al., 2010; Weidberg et al., 2011). More studies are required to clarify how ferritin is recruited to the autophagosome formation site (this is currently unknown, even for p62) and whether ferritin can be recognized by the isolation membrane.

MATERIALS AND METHODS

Plasmids

The following plasmids have been described previously: pMXs-IP-GFP-LC3, pMXs-IP-GFP-ATG5 and pMXs-IP-HA-ULK1 (Hara et al., 2008), pMRX-IP-GFP-ULK1 (Itakura et al., 2012a), pMXs-IP-GFP-ATG14 (Itakura et al., 2008), pMXs-puro-GFP-DFCP1 and pMXs-puro-GFP-WIPI-1 (Itakura and Mizushima, 2010).

Cell culture and transfection

MEFs and HeLa cells were cultured in Dulbecco's modified Eagle's medium (DMEM) supplemented with 10% fetal bovine serum and 50 μg/ml penicillin and streptomycin (regular medium) under 5% CO_2. FIP200-knockout (Gan et al., 2006), ATG9A-knockout (Saitoh et al., 2009) and ATG5-knockout MEFs (Kuma et al., 2004) were as described previously. For starvation, cells were washed with phosphate-buffered saline (PBS) and incubated in amino-acid-free DMEM without serum (starvation medium). E64d and pepstatin were purchased from Peptide Institute (Osaka, Japan). Wortmannin, bafilomycin A_1, deferoxamine mesylate salt, and ferric ammonium citrate [ammonium iron (III) citrate] were purchased from Sigma-Aldrich (St Louis, MO).

Retroviral infection and generation of stable cell lines

Stable cell lines were generated using a retroviral expression system as described previously (Hara et al., 2008; Kitamura et al., 2003). Briefly, Plat E cells (kindly provided by Toshio Kitamura, University of Tokyo, Tokyo, Japan) were transiently transfected with retroviral vectors using FuGENE HD reagent (Roche Applied Science, Mannheim, Germany). After culture for 72 h, the growth medium containing retroviruses was collected. MEFs were incubated with the collected virus-containing medium with 8 μg/ml polybrene for 24 h. Non-infected cells were removed by puromycin selection.

Antibodies

Rat monoclonal anti-GFP (GF090R) and anti-Lamp1 (1D4B) antibodies were purchased from Nacalai Tesque (Kyoto, Japan) and Abcam (Cambridge, MA), respectively. Rabbit polyclonal antibodies against LC3 (LC3#1, for immunoblotting) (Hosokawa et al., 2006), ATG9A (Itakura et al., 2012a) and ATG16L1 (Mizushima et al., 2003) have been described previously. Mouse monoclonal anti-LC3 antibody (clone LC3 1703 for immunocytochemistry and immunoelectron microscopy) was purchased from Cosmo Bio (Tokyo, Japan). Mouse monoclonal anti-HA (16B12) antibody was purchased from Covance Research Products (Richmond, CA). Guinea pig polyclonal anti-p62 antibodies were purchased from Progen (Heidelberg, Germany). Rabbit polyclonal anti-ferritin antibodies (Boehringer Ingelheim, Ingelheim am Rhein, Germany) were used for immunoelectron microscopy. A rabbit polyclonal antibody against horse spleen ferritin was purchased from

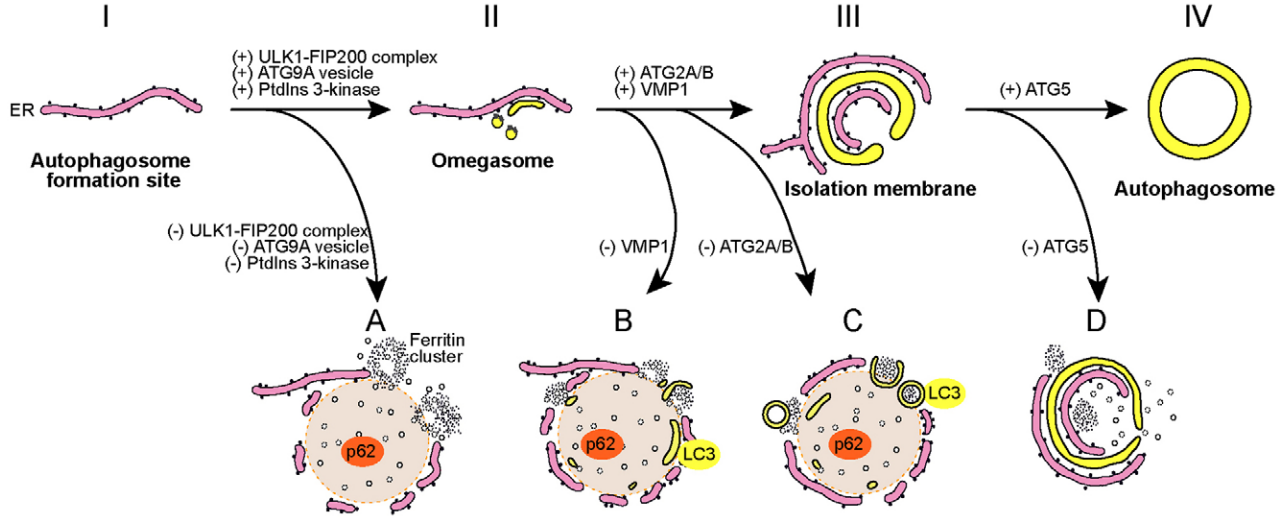

Fig. 8. Model of autophagosome biogenesis. (I) Autophagosome formation is initiated on or close to the ER by recruitment of the ULK1–FIP200 complex, ATG9A vesicles and the autophagy-specific PtdIns 3-kinase complex. Deletion of FIP200 or ATG9A, or treatment with the PtdIns 3-kinase inhibitor wortmannin, completely suppresses formation of the isolation membrane, leading to the accumulation of vesicles and selective substrates, such as p62 and ferritin clusters, near the ER (structure A). (II,III) Small isolation membranes are formed and elongate. Deletion of VMP1 or ATG2A/B inhibits elongation of this membrane. Deletion of VMP1 and ATG2A/B causes accumulation of small isolation-membrane-like structures (structure B) and small autophagosome-like structures (structure C), respectively. (IV) Elongated isolation membranes are sealed to form autophagosomes. Depletion of ATG5 likely inhibits the closure step and causes the accumulation of isolation membranes that retain association with the ER (structure D).

Sigma-Aldrich and used for immunocytochemistry. To generate antibodies against human VMP1, human VMP1 cDNA (encoding amino acid residues 1–77) was subcloned into pGEX-6p-1 (GE Healthcare, Buckinghamshire, UK). The resulting GST-fused VMP1 protein was used to immunize rabbits. Anti-HSP90 antibody was purchased from BD Biosciences (San Jose, CA).

Immunocytochemistry

Immunocytochemistry was performed as described previously (Itakura et al., 2012b). Briefly, cells grown on coverslips were washed with PBS and fixed in 4% paraformaldehyde in PBS for 10 min at 4℃. Fixed cells were permeabilized with 50 µg/ml digitonin in PBS for 5 min, blocked with 3% bovine serum albumin in PBS for 30 min, and incubated with primary antibodies for 1 h or overnight at 4℃ (for ferritin staining). After washing, cells were incubated with Alexa-Fluor-488-conjugated goat anti-rat-, anti-rabbit- or anti-mouse-IgG, Alexa-Fluor-564-conjugated goat anti-rabbit-, anti-mouse- or anti-guinea-pig-IgG, or Alexa-Fluor-660-conjugated goat anti-guinea-pig-IgG secondary antibodies (Invitrogen, Carlsbad, CA) for 30 min and examined under a fluorescence microscope (IX81; Olympus, Tokyo, Japan) equipped with a charge-coupled device camera (ORCA-ER; Hamamatsu Photonics, Hamamatsu, Japan) or a laser-scanning fluorescence microscope (FV1000, Olympus). A 60× 1.42 NA Plan Apo oil-immersion lens (Olympus) was used. Colocalization of two-color images was examined using MetaMorph image analysis software (version 7.7; Molecular Devices Japan, Tokyo, Japan). To rule out random superposition in the colocalization studies, the random overlapping ratio (%) was calculated using two-color images, one of which was artificially shifted to the right by 1 µm before merging.

Electron microscopy

Cells were cultured on collagen-coated plastic coverslips and fixed in 2.5% glutaraldehyde (TAAB, Berkshire, England) in 0.1 M sodium phosphate buffer pH 7.4 (phosphate buffer) for 2 h. The cells were washed in the same buffer five times and post-fixed in 1% osmium tetroxide (TAAB) in 0.1 M phosphate buffer for 1 h and then dehydrated and embedded in Epon 812 (TAAB) according to a standard procedure (Hara et al., 2008). Ultrathin sections were stained with uranyl acetate and lead citrate and observed under a Hitach H-7100 (Hitachi High-Technologies, Tokyo, Japan) or an FEI Tecnai G2 Spirit Bio Twin transmission electron microscope (FEI, Hillsboro, OR). For immunoelectron microscopy analysis, cells were fixed with 4% paraformaldehyde in phosphate buffer for 2 h on ice. The pre-embedding silver enhancement immunogold method was used as described previously (Yoshimori et al., 2000).

Immunoblotting

Immunoblotting was performed as described previously (Itakura et al., 2012b). Cell lysates were prepared in lysis buffer [50 mM Tris-HCl pH 7.5, 150 mM NaCl, 1 mM EDTA, 1% Triton X-100, 1 mM phenylmethanesulfonyl fluoride, 1 mM Na_3VO_4 and protease inhibitor cocktail (Complete EDTA-free protease inhibitor; Roche Diagnostics)]. The lysates were separated by SDS-PAGE and transferred to Immunobilon-P polyvinylidene difluoride membranes (Millipore, Billerica, MA). Immunoblot analysis was performed with the indicated antibodies and visualized with SuperSignal West Pico chemiluminescent substrate (Pierce Chemical, Rockford, IL).

RNA interference

Stealth RNAi oligonucleotides were used for siRNA experiments (Invitrogen). The following sequences were used: human ATG9A siRNA antisense, 5′-AACCAGUGCCACCAUGUAGUUCUGG-3′; sense, 5′-CCAGAACUACAUGGTGGCACUGGTT-3′; human ferritin heavy polypeptide 1 siRNA antisense, 5′-AGUCACUACUGGAACUGC-ACAAACU-3′; sense, 5′-AGUUUGUGCAGUUCCAGUAGUGACU-3′; human ferritin light polypeptide 1 siRNA antisense, 5′-GCAAAGU-AAUAGGGCUUCUGCCUAA-3′; sense, 5′-UUAGGCAGAAGCCCUA-UUACUUUGC-3′; human FIP200 siRNA antisense, 5′- UUUCUUGGCA-ACUUCAUACAUUUCC-3′; sense, 5′-GGAAAUGUAUGAAGUUGCCA-AGAAA-3′; human ATG5 siRNA antisense, 5′-AAACAAGUUGGA-AUUCGUCCAAACC-3′; sense, 5′-GGUUUGGACGAAUUCCAACUUG-UUU-3′; and luciferase siRNA antisense, 5′-AAUUAAGUCCGCUUC-UAAGGUUUCC-3′; sense, 5′-CGCGGUCGGUAAAGUUGUUCCAUUU-3′. The siRNA oligonucleotides for human VMP1 (Itakura and Mizushima, 2011), ATG2A and ATG2B (Velikkakath et al., 2012) have been reported previously. The Stealth RNAi oligonucleotides were transfected into cells using Lipofectamine RNAi MAX (Invitrogen) according to the manufacturer's protocol. After 2 days, the cells were again transfected with the same siRNA and cultured for an additional 4 days before analysis.

Flow cytometry

Autophagic flux was measured using flow cytometry as reported previously (Shvets et al., 2008). Cells stably expressing GFP–LC3 were harvested with 0.05% trypsin-EDTA and washed with ice-cold PBS. Total cellular GFP–LC3 signals were directly measured using an EC800 flow cytometry analyzer (Sony, Tokyo, Japan), and data were analyzed using Kaluza software (Beckman Coulter, Brea, CA).

Acknowledgements

We thank Jun-Lin Guan (University of Cincinnati, Cincinnati, USA) for providing FIP200-knockout MEFs and Tatsuya Saitoh and Shizuo Akira (Osaka University, Osaka, Japan) for providing ATG9A-knockout MEFs. We thank Kazuhiro Iwai (Kyoto University, Kyoto, Japan) for helpful discussion and Folma Buss (University of Cambridge, Cambridge, UK) for constant encouragement.

Competing interests

The authors declare no competing interests.

Author contributions

C. K.-I. performed electron microscopy, I. K.-H. and E. I. performed immunofluorescence microscopy and biochemical analysis, C. K.-I. and N.M. conceived the experiments. All authors analyzed the data. C. K.-I. and N.M. wrote the paper, and I. K.-H. and E. I. edited it.

Funding

This work was supported in part by the Funding Program for Next Generation World-Leading Researchers [grant number LS043]; and Japan Society for the Promotion of Science (JSPS) KAKENHI Grants-in-Aid for Scientific Research on Innovative Areas [grant number 25111005] to N.M.; and grants for a research fellowship of the JSPS for Young Scientists (to E.I.); and Supporting Positive Activities for Female Researchers (to I.K.-H.).

Supplementary material

Supplementary material available online at
http://jcs.biologists.org/lookup/suppl/doi:10.1242/jcs.156034/-/DC1

References

Arosio, P., Ingrassia, R. and Cavadini, P. (2009). Ferritins: a family of molecules for iron storage, antioxidation and more. *Biochim. Biophys. Acta* **1790**, 589-599.
Asano, T., Komatsu, M., Yamaguchi-Iwai, Y., Ishikawa, F., Mizushima, N. and Iwai, K. (2011). Distinct mechanisms of ferritin delivery to lysosomes in iron-depleted and iron-replete cells. *Mol. Cell. Biol.* **31**, 2040-2052.
Axe, E. L., Walker, S. A., Manifava, M., Chandra, P., Roderick, H. L., Habermann, A., Griffiths, G. and Ktistakis, N. T. (2008). Autophagosome formation from membrane compartments enriched in phosphatidylinositol 3-phosphate and dynamically connected to the endoplasmic reticulum. *J. Cell Biol.* **182**, 685-701.
Birgisdottir, A. B., Lamark, T. and Johansen, T. (2013). The LIR motif – crucial for selective autophagy. *J. Cell Sci.* **126**, 3237-3247.
Choi, A. M., Ryter, S. W. and Levine, B. (2013). Autophagy in human health and disease. *N. Engl. J. Med.* **368**, 651-662.
De Domenico, I., Ward, D. M. and Kaplan, J. (2009). Specific iron chelators determine the route of ferritin degradation. *Blood* **114**, 4546-4551.
Gan, B., Peng, X., Nagy, T., Alcaraz, A., Gu, H. and Guan, J. L. (2006). Role of FIP200 in cardiac and liver development and its regulation of TNFalpha and TSC-mTOR signaling pathways. *J. Cell Biol.* **175**, 121-133.
Ghadially, F. N. (1975). *Ultrastructural Pathology of the Cell*. London: Butterworth-Heinemann.
Gregory, A. and Hayflick, S. J. (2011). Genetics of neurodegeneration with brain iron accumulation. *Curr. Neurol. Neurosci. Rep.* **11**, 254-261.
Haack, T. B., Hogarth, P., Kruer, M. C., Gregory, A., Wieland, T., Schwarzmayr, T., Graf, E., Sanford, L., Meyer, E., Kara, E. et al. (2012). Exome sequencing reveals de novo WDR45 mutations causing a phenotypically distinct, X-linked dominant form of NBIA. *Am. J. Hum. Genet.* **91**, 1144-1149.

Haack, T. B., Hogarth, P., Gregory, A., Prokisch, H. and Hayflick, S. J. (2013). BPAN: the only X-linked dominant NBIA disorder. *Int. Rev. Neurobiol.* **110**, 85-90.
Hara, T., Takamura, A., Kishi, C., Iemura, S., Natsume, T., Guan, J. L. and Mizushima, N. (2008). FIP200, a ULK-interacting protein, is required for autophagosome formation in mammalian cells. *J. Cell Biol.* **181**, 497-510.
Heynen, M. J. and Verwilghen, R. L. (1982). A quantitative ultrastructural study of normal rat erythroblasts and reticulocytes. *Cell Tissue Res.* **224**, 397-408.
Hosokawa, N., Hara, Y. and Mizushima, N. (2006). Generation of cell lines with tetracycline-regulated autophagy and a role for autophagy in controlling cell size. *FEBS Lett.* **580**, 2623-2629.
Itakura, E. and Mizushima, N. (2010). Characterization of autophagosome formation site by a hierarchical analysis of mammalian Atg proteins. *Autophagy* **6**, 764-776.
Itakura, E. and Mizushima, N. (2011). p62 Targeting to the autophagosome formation site requires self-oligomerization but not LC3 binding. *J. Cell Biol.* **192**, 17-27.
Itakura, E., Kishi, C., Inoue, K. and Mizushima, N. (2008). Beclin 1 forms two distinct phosphatidylinositol 3-kinase complexes with mammalian Atg14 and UVRAG. *Mol. Biol. Cell* **19**, 5360-5372.
Itakura, E., Kishi-Itakura, C., Koyama-Honda, I. and Mizushima, N. (2012a). Structures containing Atg9A and the ULK1 complex independently target depolarized mitochondria at initial stages of Parkin-mediated mitophagy. *J. Cell Sci.* **125**, 1488-1499.
Itakura, E., Kishi-Itakura, C. and Mizushima, N. (2012b). The hairpin-type tail-anchored SNARE syntaxin 17 targets to autophagosomes for fusion with endosomes/lysosomes. *Cell* **151**, 1256-1269.
Johansen, T. and Lamark, T. (2011). Selective autophagy mediated by autophagic adapter proteins. *Autophagy* **7**, 279-296.
Kageyama, S., Omori, H., Saitoh, T., Sone, T., Guan, J. L., Akira, S., Imamoto, F., Noda, T. and Yoshimori, T. (2011). The LC3 recruitment mechanism is separate from Atg9L1-dependent membrane formation in the autophagic response against Salmonella. *Mol. Biol. Cell* **22**, 2290-2300.
Kidane, T. Z., Sauble, E. and Linder, M. C. (2006). Release of iron from ferritin requires lysosomal activity. *Am. J. Physiol.* **291**, C445-C455.
Kitamura, T., Koshino, Y., Shibata, F., Oki, T., Nakajima, H., Nosaka, T. and Kumagai, H. (2003). Retrovirus-mediated gene transfer and expression cloning: powerful tools in functional genomics. *Exp. Hematol.* **31**, 1007-1014.
Koyama-Honda, I., Itakura, E., Fujiwara, T. K. and Mizushima, N. (2013). Temporal analysis of recruitment of mammalian ATG proteins to the autophagosome formation site. *Autophagy* **9**, 1491-1499.
Kuma, A., Hatano, M., Matsui, M., Yamamoto, A., Nakaya, H., Yoshimori, T., Ohsumi, Y., Tokuhisa, T. and Mizushima, N. (2004). The role of autophagy during the early neonatal starvation period. *Nature* **432**, 1032-1036.
Lamb, C. A., Yoshimori, T. and Tooze, S. A. (2013). The autophagosome: origins unknown, biogenesis complex. *Nat. Rev. Mol. Cell Biol.* **14**, 759-774.
Levine, B. and Kroemer, G. (2008). Autophagy in the pathogenesis of disease. *Cell* **132**, 27-42.
Mancias, J. D., Wang, X., Gygi, S. P., Harper, J. W. and Kimmelman, A. C. (2014). Quantitative proteomics identifies NCOA4 as the cargo receptor mediating ferritinophagy. *Nature* **509**, 105-109.
Mizushima, N. and Komatsu, M. (2011). Autophagy: renovation of cells and tissues. *Cell* **147**, 728-741.
Mizushima, N., Yamamoto, A., Hatano, M., Kobayashi, Y., Kabeya, Y., Suzuki, K., Tokuhisa, T., Ohsumi, Y. and Yoshimori, T. (2001). Dissection of autophagosome formation using Apg5-deficient mouse embryonic stem cells. *J. Cell Biol.* **152**, 657-668.
Mizushima, N., Kuma, A., Kobayashi, Y., Yamamoto, A., Matsubae, M., Takao, T., Natsume, T., Ohsumi, Y. and Yoshimori, T. (2003). Mouse Apg16L, a novel WD-repeat protein, targets to the autophagic isolation membrane with the Apg12-Apg5 conjugate. *J. Cell Sci.* **116**, 1679-1688.
Mizushima, N., Yoshimori, T. and Levine, B. (2010). Methods in mammalian autophagy research. *Cell* **140**, 313-326.
Mizushima, N., Yoshimori, T. and Ohsumi, Y. (2011). The role of Atg proteins in autophagosome formation. *Annu. Rev. Cell Dev. Biol.* **27**, 107-132.
Nakatogawa, H., Suzuki, K., Kamada, Y. and Ohsumi, Y. (2009). Dynamics and diversity in autophagy mechanisms: lessons from yeast. *Nat. Rev. Mol. Cell Biol.* **10**, 458-467.
Noda, N. N., Ohsumi, Y. and Inagaki, F. (2010). Atg8-family interacting motif crucial for selective autophagy. *FEBS Lett.* **584**, 1379-1385.
Ollinger, K. and Roberg, K. (1997). Nutrient deprivation of cultured rat hepatocytes increases the desferrioxamine-available iron pool and augments the sensitivity to hydrogen peroxide. *J. Biol. Chem.* **272**, 23707-23711.
Orsi, A., Razi, M., Dooley, H. C., Robinson, D., Weston, A. E., Collinson, L. M. and Tooze, S. A. (2012). Dynamic and transient interactions of Atg9 with autophagosomes, but not membrane integration, are required for autophagy. *Mol. Biol. Cell* **23**, 1860-1873.
Saitoh, T., Fujita, N., Hayashi, T., Takahara, K., Satoh, T., Lee, H., Matsunaga, K., Kageyama, S., Omori, H., Noda, T. et al. (2009). Atg9a controls dsDNA-driven dynamic translocation of STING and the innate immune response. *Proc. Natl. Acad. Sci. USA* **106**, 20842-20846.
Saitsu, H., Nishimura, T., Muramatsu, K., Kodera, H., Kumada, S., Sugai, K., Kasai-Yoshida, E., Sawaura, N., Nishida, H., Hoshino, A. et al. (2013). De novo mutations in the autophagy gene WDR45 cause static encephalopathy of childhood with neurodegeneration in adulthood. *Nat. Genet.* **45**, 445-449, e1.
Shvets, E., Fass, E. and Elazar, Z. (2008). Utilizing flow cytometry to monitor autophagy in living mammalian cells. *Autophagy* **4**, 621-628.
Sou, Y. S., Waguri, S., Iwata, J., Ueno, T., Fujimura, T., Hara, T., Sawada, N., Yamada, A., Mizushima, N., Uchiyama, Y. et al. (2008). The Atg8 conjugation system is indispensable for proper development of autophagic isolation membranes in mice. *Mol. Biol. Cell* **19**, 4762-4775.
Suzuki, K., Kubota, Y., Sekito, T. and Ohsumi, Y. (2007). Hierarchy of Atg proteins in pre-autophagosomal structure organization. *Genes Cells* **12**, 209-218.
Tian, Y., Li, Z., Hu, W., Ren, H., Tian, E., Zhao, Y., Lu, Q., Huang, X., Yang, P., Li, X. et al. (2010). C. elegans screen identifies autophagy genes specific to multicellular organisms. *Cell* **141**, 1042-1055.
Tooze, S. A. and Yoshimori, T. (2010). The origin of the autophagosomal membrane. *Nat. Cell Biol.* **12**, 831-835.
Uemura, T., Yamamoto, M., Kametaka, A., Sou, Y. S., Yabashi, A., Yamada, A., Annoh, H., Kametaka, S., Komatsu, M. and Waguri, S. (2014). A cluster of thin tubular structures mediates transformation of the endoplasmic reticulum to autophagic isolation membrane. *Mol. Cell. Biol.* **34**, 1695-1706.
Velikkakath, A. K., Nishimura, T., Oita, E., Ishihara, N. and Mizushima, N. (2012). Mammalian Atg2 proteins are essential for autophagosome formation and important for regulation of size and distribution of lipid droplets. *Mol. Biol. Cell* **23**, 896-909.
Watt, R. K. (2011). The many faces of the octahedral ferritin protein. *Biometals* **24**, 489-500.
Weidberg, H., Shvets, E. and Elazar, Z. (2011). Biogenesis and cargo selectivity of autophagosomes. *Annu. Rev. Biochem.* **80**, 125-156.
Yoshimori, T., Yamagata, F., Yamamoto, A., Mizushima, N., Kabeya, Y., Nara, A., Miwako, I., Ohashi, M., Ohsumi, M. and Ohsumi, Y. (2000). The mouse SKD1, a homologue of yeast Vps4p, is required for normal endosomal trafficking and morphology in mammalian cells. *Mol. Biol. Cell* **11**, 747-763.